JOURNAL OF SOLID STATE CHEMISTRY 114, 435–441 (1995)

Structure Determination of a Trilayer Misfit Compound $(Gd_\varepsilon Sn_{1-\varepsilon}S)_{1.16}(NbS_2)_3$

Laura M. Hoistad, Alain Meerschaut, Philippe Bonneau, and Jean Rouxel

Institut des Matériaux de Nantes, UMR-CNRS 110, Laboratoire de Chimie des Solides, 2 rue de la Houssinière, 44072 Nantes Cedex 02, France

Received April 8, 1994; accepted May 25, 1994

We present the synthesis, single crystal refinement, and powder refinement of a new misfit compound, $(Gd_\varepsilon Sn_{1-\varepsilon}S)_{1.16}(NbS_2)_3$. The single crystal structure was determined using a composite approach comprised of three refinement steps. The powder refinement was done using four-dimensional space with one modulation vector to model the incommensurate axis. The structure consists of three consecutive layers of NbS_2 followed by a layer of MS.

INTRODUCTION

In the past few years there has been considerable development in the family of compounds known as the misfit layered compounds (1). The misfit compounds are composite materials built of alternating layers of MX and TX_2 (M = Sn, Pb, Bi, or rare earth; T = early transition metal; and X = S or Se). A general structural formulation of $(MX)_n(TX_2)_m$ for the misfit compounds arises from this alternation of the two different layers. The MX layer has a distorted rock-salt structure which is two atoms thick. The TX_2 part exhibits the same kinds of layers found for the layered transition metal dichalcogenides.

The first type of misfit compounds synthesized were those where $m = 1$ (monolayer type). The regular stacking of the two types of layers results in a common c parameter for both sublattices. Each of the two sublattices have their own a and b in-plane parameters. In all the known monolayer-type compounds, the b parameters for the two sublattices are identical but the ratio of the two a parameters is expressed by an irrational number. This misfit between the two slabs results in a chemical formulation of $(MX)_{1+x}(TX_2)$ with $0.0 < x < 0.3$ depending on the size of M.

Recently several new misfit compounds where $m = 2$ have been synthesized (2). These bilayer misfit compounds contain a van der Waals gap between the two successive TX_2 layers in the TX_2 portion of the structure. In addition, the stacking mode of the TX_2 layers has a discernible polytype like those found for the pure layered dichalcogenides. Figure 1 illustrates the structures of "$PbNb_2Se_5$" and the orthorhombic and monoclinic forms of "$PbNb_2S_5$." In the orthorhombic form of "$PbNb_2S_5$," the NbS_2 part adopts a 3R-type stacking which, in fact, is $\frac{2}{3}$ of unit cell of 3R–NbS_2 (Fig. 1a) (2a). The monoclinic form of "$PbNb_2S_5$" also has the 3R stacking but the orientation of the $(NbS_2)_2$ slabs on either side of the PbS layer is the same (Fig. 1b), while in the orthorhombic form the orientation is reversed (2b). On the other hand, in "$PbNb_2Se_5$" the $NbSe_2$ layers adopt the $2H_a$–$NbSe_2$ structure (Fig. 1c) (2c).

In the bilayer misfit compounds, a direct relationship can be drawn between the electronic properties and the observed polytype. The misfit compounds with the 2H polytype are superconducting, while the compounds with a 3R polytype are not. A "trilayer" compound would provide an additional piece of information regarding the change of properties with respect to polytype. There has been a previous report of a trilayer selenide misfit compound (3). This paper illustrated the potential of modifying the properties of the material with increased staging of the $NbSe_2$ portion. However, due to the lack of good crystals, the single crystal structure was not determined, thus making it difficult to draw any conclusions on the question of polytype versus observed properties. In this paper we will discuss the synthesis and single crystal refinement of a new misfit compound $(Gd_\varepsilon Sn_{1-\varepsilon}S)_{1.16}(NbS_2)_3$. This is the first single crystal structure of a misfit material with three adjacent layers of TX_2.

EXPERIMENTAL

Synthesis

Mixed Sn–Gd trilayer misfit compounds were obtained as a side product in the course of studies aimed to dope Sn into the highly magnetic GdS layers (4). Powder diffraction studies showed the presence of a trilayer compound only when the concentration of Gd in the layer was very low. (We have succeeded in obtaining just the

0022-4596/95 $6.00

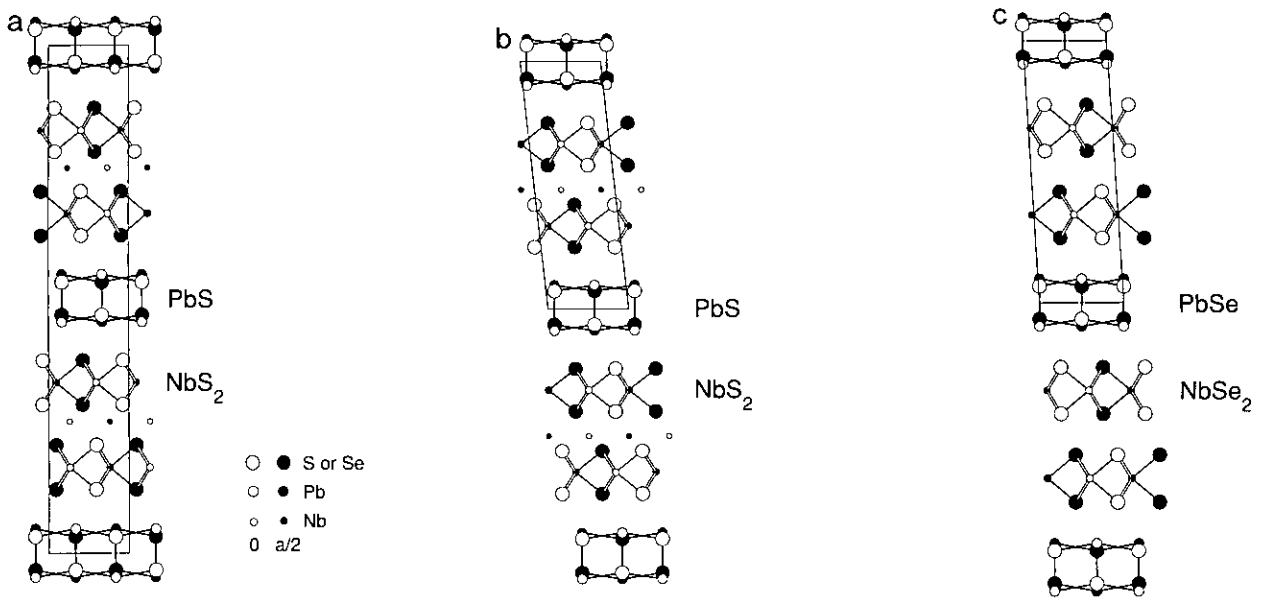

FIG. 1. The projection of (a) "$PbNb_2S_5$" orthorhombic, (b) "$PbNb_2S_5$" monoclinic, and (c) "$PbNb_2Se_5$" down the a axis. These structures are built by stacking two layers of NbX_2 followed by one layer of PbX. The NbX_2 portion in both the "$PbNb_2S_5$" compounds has $\frac{3}{4}$ of the 3R polytype (see Fig. 3). However, in "$PbNb_2Se_5$" the NbX_2 portion has the $2H_a$ polytype. Both of the "$PbNb_2S_5$" forms also have supplementary Nb in the van der Waals gap. The difference between the monoclinic and the orthorhombic forms is the orientation of the $(NbS_2)_2$ blocks on either side of the PbS layer. In the orthorhombic form, the orientation changes, while in the monoclinic form the orientation remains the same.

trilayer compound from the elements Sn, Nb, and S.) The nominal purities were S 99.999% (from Fluka), Nb 99.8% (from Alfa), and Sn 99% (from Koch-Light). The source of the Gd was Gd_2S_3 which was previously prepared by the sulfurization of Gd_2O_3 (99.9% purity from Strem Chemicals) with H_2S. Each sample was sealed in evacuated quartz ampules and heated at a rate of approximately 10°C/hr to 1050°C. The samples were held at 1050°C for 7 to 14 days. The furnace was then cooled to room temperature within 24 hr. We ground and again annealed the samples at 1050°C for 14 days. A small amount of I_2 was added for the second annealing to aid crystallization. Semiquantitative chemical analyses were performed using an electron microprobe (TRACOR dispersive energy model) mounted on a scanning electron microscope. Analysis on several crystals revealed that the Gd concentration ranged from 4 to 8% with respect to the Nb concentration ($0.12 < \varepsilon < 0.24$). The stoichiometric amount of Gd in the samples was $\varepsilon = 0.15$. The structural study (see below) showed that the stabilization of the observed three-layered structure could be due to a slight excess of Nb between the NbS_2 layers. Following this idea, preparations for a pure "$SnNb_3S_7$" trilayer phase were attempted by adding a slight excess of Nb. These syntheses were successful as evidenced by powder diffraction. However at this time we have not been able to obtain good single crystals.

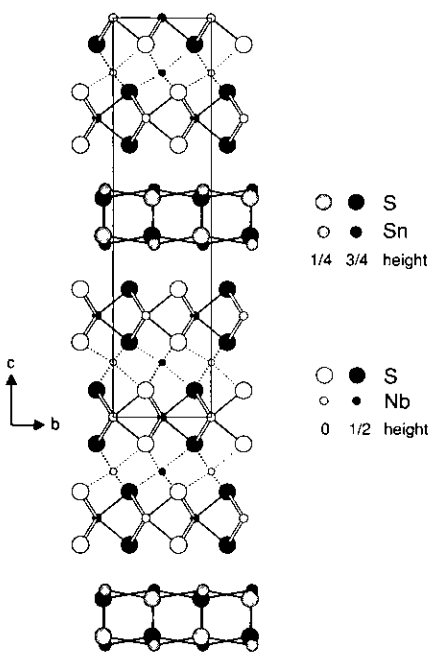

FIG. 2. The projection of $(SnS)_{1.16}(NbS_2)_3$ along the misfit axis. The $[(NbS_2)_3]$ substructure is a portion of either the $4H_a$ or the 3R polytype (see Fig. 3). The $[(NbS_2)_3$ block is followed by an [SnS] block. The Sn and S have a distorted rock-salt structure.

Powder Refinement

The room temperature powder spectrum was recorded on an INEL powder diffractometer. The powder spectrum

TABLE 1
Powder Refinement of $(Gd_\epsilon Sn_{1-\epsilon}S)_{1.16}(NbS_2)_3$

h k l m	d_{obs} (Å)	d_{calc} (Å)	I_{obs}	h k l m	d_{obs} (Å)	d_{calc} (Å)	I_{obs}	h k l m	d_{obs} (Å)	d_{calc} (Å)	I_{obs}
0 0 3 0	7.857	7.863	3	0 1 6 1	2.3219	2.3225	100	0 0 15 0	1.5724	1.5725	6
0 0 4 0	5.887	5.897	66	0 2 7 0	2.1887	2.1887	15	0 3 7 1	1.4899	1.4905	4
0 0 5 0	4.711	4.718	8	0 1 7 1	2.1887	2.1887	15	0 0 7 2	1.4899	1.4905	4
0 0 6 0	3.926	3.931	15	0 0 11 0	2.1436	2.1444	10	0 0 16 0	1.4748	1.4743	82
1 1 2 0	3.826	3.827	15	0 2 8 0	2.0594	2.0598	24	0 2 14 0	1.4540	1.4541	10
1 1 3 0	3.595	3.598	6	0 1 8 1	2.0594	2.0597	24	0 1 14 1	1.4540	1.4541	10
0 0 7 0	3.367	3.370	24	2 2 0 0	2.0229	2.0232	13	0 4 1 0	1.4365	1.4366	3
0 2 0 0	2.8775	2.8786	31	2 2 2 0	1.9943	1.9941	2	0 2 1 2	1.4365	1.4366	3
0 1 0 1	2.8775	2.8786	31	0 0 12 0	1.9657	1.9567	42	0 4 2 0	1.4286	1.4287	6
0 2 1 0	2.8574	2.8574	16	0 2 9 0	1.9380	1.9380	9	0 2 2 2	1.4286	1.4286	6
0 1 1 1	2.8574	2.8574	16	0 1 9 1	1.9380	1.9380	9	0 4 4 0	1.3984	1.3982	3
2 0 0 0	2.8436	2.8442	7	0 2 10 0	1.8248	1.8245	20	0 2 4 2	1.3984	1.3982	3
2 0 1 0	2.8259	2.8237	19	0 1 10 1	1.8248	1.8245	20	0 4 6 0	1.3516	1.3516	10
0 2 2 0	2.7967	2.7965	80	1 1 12 0	1.7680	1.7681	3	0 2 6 2	1.3516	1.3515	10
0 1 2 1	2.7967	2.7964	80	0 3 0 1	1.6617	1.6619	23	0 2 16 0	1.3124	1.3122	7
0 2 3 0	2.7030	2.7031	4	0 0 0 2	1.6617	1.6619	23	0 1 16 1	1.3124	1.3122	7
0 1 3 1	2.7030	2.7030	4	0 3 1 1	1.6575	1.6578	8	0 4 8 0	1.2936	1.2934	6
0 0 9 0	2.6207	2.6209	15	0 0 1 2	1.6575	1.6578	8	0 2 8 2	1.2936	1.2934	6
0 2 4 0	2.5874	2.5869	27	0 3 2 1	1.6455	1.6457	4	0 3 12 1	1.2693	1.2691	8
0 1 4 1	2.5874	2.5868	27	0 0 2 2	1.6455	1.6456	4	0 0 12 2	1.2693	1.2691	8
0 2 5 0	2.4565	2.4573	15	0 3 3 1	1.6259	1.6260	3	0 4 9 0	1.2618	1.2616	2
0 1 5 1	2.4565	2.4572	15	0 0 3 2	1.6259	1.6260	3	0 2 9 2	1.2618	1.2615	2
0 0 10 0	2.3577	2.3588	14	0 3 4 1	1.5995	1.5996	16	0 4 10 0	1.2288	1.2286	8
0 2 6 0	2.3219	2.3226	100	0 0 4 2	1.5995	1.5996	16	0 2 10 2	1.2288	1.2286	8

of the bulk sample from the Gd–Sn preparation confirmed the presence of one major product with slight contamination of NbS_2. There was no significant line broadening found in the powder spectrum even though the microprobe analysis indicated a variation in chemical composition. The powder refinement was performed using the U-fit program with one modulation vector (5). The misfit axis can be modeled by modulation vector with a component in the misfit direction. The component of the modulation, α, is equal to $a_{[MS]}/a_{[NbS_2]}$. The advantage to a powder refinement performed in this way is that the commensurate axes (b and c) are equal for the two sublattices i.e., $b_{[MS]} = b_{[NbS_2]}$ and $c_{[MS]} = c_{[NbS_2]}$. This may not be the case if the refinement is done using a composite approach with two separate refinements, one for the NbS_2 reflections and one for the MS reflections. The indexing for each reflection requires four indices h, k, l, and m, where h, k, and l correspond to the hkl indexing of the MS substructure and m, k, and l correspond to the hkl indexing in the NbS_2 substructure. Each reflection in the spectrum falls into one of three categories:

$hkl0$, reflections of the MS substructure,

$0klm$, reflections of the NbS_2 substructure,

$0kl0$, reflections common to both substructures.

Table 1 lists the observed and calculated d spacings along with the observed intensity of each reflection. The unit cell parameters refined to a = 5.688(1) Å, b = 5.7572(4) Å, and c = 23.588(2) Å. These values correspond to the cell parameters of the MS substructure. The α component of the modulation vector refined to a value of 1.7114(4) which corresponds to 3.3237 Å for the a cell parameter of the NbS_2 part. The a and b parameters correspond closely to the cell parameters found in $(SnS)_{1.16}NbS_2$ of $a_{[MS]}$ = 5.673 Å, b = 5.751 Å, and $a_{[NbS_2]}$ = 3.321 Å (6). The cell parameters for the Gd analog are more contracted with $a_{[MS]}$ = 5.518 Å, b = 5.708 Å, and $a_{[NbS_2]}$ = 3.311 Å (1). The comparison of the in-plane parameters suggests that there is no ordering of the Gd in the MS layer of $(Gd_\epsilon Sn_{1-\epsilon}S)_{1.16}(NbS_2)_3$.

Single Crystal Refinement

For the single crystal refinement, a crystal obtained from the Gd–Sn preparation was used. We determined that the crystal had orthorhombic symmetry from the Bragg and Weissenberg studies. The single crystal data were collected on an Enraf–Nonius CAD4 diffractometer. A composite approach was used for the single crystal refinement. The refinement was conducted in three parts, NbS_2, MS, and the common part. Two sets of data are required, one set for the NbS_2 substructure and a second set for the MS substructure. The common part of the structure was refined using the $0kl$ reflections which are

TABLE 2
Data Collections and Refinements Summary for $(Gd_eSn_{1-e}S)_{1.16}(NbS_2)_3$

Crystal data			
Empirical formula	$Sn_{1.16}Nb_{3.22}S_{7.16}$ (from refinement)		
Formula weight	655.89 g/mole		
Crystal color and habit	Black platelet		
Crystal system	Orthorhombic		
	[NbS_2] part	[SnS] part	Common part
Data collection			
Diffractometer	Enraf-Nonius CAD4	Enraf-Nonius CAD4	Enraf-Nonius CAD4
Radiation type	Mo$K\alpha$, λ = 0.71073 Å Graphite monochrometer	Mo$K\alpha$, λ = 0.71073 Å Graphite monochrometer	Mo$K\alpha$, λ = 0.71073 Å Graphite monochrometer
Temperature	Ambient	Ambient	Ambient
θ Scan range	1.5°–35°	1.5°–35°	1.5°–35°
Scan mode	ω	ω	ω
Scan width	1.0 + 0.35 tan θ	1.0 + 0.35 tan θ	1.0 + 0.35 tan θ
Octants used (max/min)	h, 5/0; k, 9/0; l, 76/0	h, 9/−9; k, 9/0; l, 76/0	h, 5/0; k, 9/0; l, 76/0
Number of data collected	1245	3728	1245
Unit cell dimensions			
a	3.3237(3) Å	5.688(8) Å	—
b	5.7572(4) Å	5.7572(4) Å	5.7572(4) Å
c	23.588(2) Å	23.588(2) Å	23.588(2) Å
α	90.0°	90.0°	90.0°
β	90,0°	90.0°	90.0°
γ	90.0°	90.0°	90.0°
Volume	451.4 Å^3	781.3 Å^3	—
Solution and refinement			
Refinement method	Full-matrix least-squares	Full-matrix least-squares	Full-matrix least-squares
Space group	$Cm2m$ (No. 38)	$Cm2a$ (No. 39)	$Cm2m$ (No. 38)
General positions	xyz, $\bar{x}yz$,	xyz, $\bar{x}y\bar{z}$,	xyz, $\bar{x}yz$,
+(0,0,0); ($\frac{1}{2}$,$\frac{1}{2}$,0)	$xy\bar{z}$, $\bar{x}y\bar{z}$	$\frac{1}{2}+xyz$, $\frac{1}{2}-xyz$	$xy\bar{z}$, $\bar{x}y\bar{z}$
Weighting scheme	Unit weights	Unit weights	Unit weights
Absorption correction (abs_{min}/abs_{max})	0.865/1.276	0.111/1.279	0.854/1.999
Number of refined reflections	413	192	140
Number of parameters	18	9	12
$R = \Sigma(\|\|F_o\| - \|F_c\|\|)/\Sigma\|F_o\|$	0.03753	0.05233	0.05168
$R_w = \Sigma_w(\|\|F_o\| - \|F_c\|\|)^2/\Sigma_w\|F_o\|^2$	0.04039	0.06351	0.05361
Residual electron density	±0.680 e^-/Å^3	±0.507 e^-/Å^3	±0.252 e^-/Å^3

found in both substructures. Both sets of data were collected from the same crystal. The intensities of both sets were corrected for Lorentz and polarization effects. There was no significant decay in intensity during the data collection. The MOLEN refinement package (7) was used for the refinement. All three refinements had an internal absorption correction applied using the DIFABS program (8) once all atoms had been located and refined isotropically. Table 2 lists the details of the data collections and refinements.

NbS_2 Part

From the observed systematic condition (hkl, $h + k = 2n$), we determined the space group was $Cm2m$ (No. 38). The data used for the refinement were those unique to the NbS_2 substructure. All the $0kl$ reflections are common to both substructures and therefore not used in this part of the refinement. The Nb and S positions were found via a Patterson map. The refinement reliability factors before an internal absorption correction were R = 8.17% and R_w = 9.47% for 413 reflections ($I \geq 3.0\sigma I$) and 14 variables. There was a residual peak (6.26 e^-/Å^3) in the Fourier difference map which corresponded to the octahedral holes located in the van der Waals gap. This peak was attributed to supplementary Nb occupying these sites. Extra Nb in the van der Waals gap has been found for other bilayer misfit compounds as well as some pure transition metal dichalcogenides (2b). The supplementary Nb

TABLE 3
Positional Parameters and Estimated Standard Deviations from the Refinement of the [NbS_2] Part (Space Group *Cm2m*)

Atom	Site	x	y	z	B_{iso}	sof[a]
Nb1	2*a*	0	0	0	0.45(2)	1.00
S1	4*c*	0	0.3336(7)	0.0662(1)	0.54(3)	1.00
Nb2	4*c*	0	0.3330(3)	0.25269(5)	0.53(1)	1.00
S2	4*c*	½	0.1668(6)	0.3190(1)	0.73(4)	1.00
S3	4*c*	½	1.1670(6)	0.1869(1)	0.81(4)	1.00
Nb supp	4*c*	0	0.002(2)	0.1368(4)	0.8(1)	0.11(2)

[a] The definition of site occupancy factor (sof) is the average population of that site.

(marked Nb supp) was added to the refinement. We fixed the site occupancy at 10% and refined only the positional parameters and the isotropic thermal factor. The refinement then yielded reliability factors of $R = 6.00\%$ and $R_w = 7.13\%$ for three more parameters than in the refinement without the supplementary Nb. The supplementary Nb does indeed significantly lower the R factors. At this stage of the refinement, an internal absorption correction was performed using the DIFABS program. At this point, we refined the occupancy of the supplementary Nb which refined to 11.4%. The R factors of the final refinement were $R = 3.75\%$ and $R_w = 4.04\%$. Table 3 lists the final positional parameters and isotropic thermal parameters.

MS Part

As with the NbS_2 part, the 0*kl* reflections were not used for the refinement of the *M*S substructure. The positions of Sn and S were determined from a Patterson map. The space group used for this refinement was *Cm2a* (No. 39) due to the extra systematic condition ($hk0$, $h = 2n$). After the refinement of the positional parameters and the isotropic thermal factors, we attempted to place Gd on the Sn sites. The occupancy of the Gd and the Sn were constrained to one another to achieve a statistical distribution of Sn and Gd in the layer. The occupancy of the Gd went to zero upon refinement of the Gd and Sn occupancies. The difference of electron density between the Sn and the Gd should allow for the refinement of the occupancies. Assuming there is no Gd present in the structure, we refined the Sn anisotropically. After the internal absorption correction was applied, the final reliability factors were $R = 5.23\%$ and $R_w = 6.35\%$ for 192 reflections ($I \geq 3.0\sigma I$) and nine variables. At this point, we again attempted to place a statistical amount of Gd on the Sn sites. The same result was achieved with the site occupancy of the Gd refining to less than 1%. Recall that the Gd concentration was not uniform from crystal to crystal in the microprobe analyses and it may have been possible that the amount of Gd contained in the crystal used for data collection was extremely low. Unfortunately, the crystal was lost before verification of its concentration. The most notable peak in the Fourier difference map was located at (0.0, 0.25, 0.5) with an electron density of 0.507 $e^-.Å^{-3}$. Table 4 lists the final positional parameters and anisotropic thermal factors of Sn.

Common Part

For this refinement the 0*kl* reflections from the NbS_2 data part were used. Recall that the 0*kl* reflections are common to both substructures. The space group *Cm2m* (No. 38) was also used for the refinement of the common part. The atomic positions for the NbS_2 part were kept fixed to the values found in the separate refinement. Only the thermal factors were allowed to be refined. The SnS layer was refined relative to the fixed NbS_2 portion. S4 was constrained to the Sn1 such that the differences in the y and z positional parameters remained fixed to the differences found in the separate refinement of the [SnS] block. The y and z positional parameters for the Sn were refined along with the thermal factors and the occupancies. The final reliability factors were $R = 5.17\%$ and $R_w = 5.36\%$ for 140 reflections ($I \geq 3.0\sigma I$) and 12 refined parameters. The most significant peak in the Fourier difference map was located at (0.15, 0.23, 0.45) with a density of 0.25 $e^-.Å^{-3}$. The final parameters are listed in Table 5.

RESULTS AND DISCUSSION

Figure 3 shows the projection of $(SnS)_{1.16}(NbS_2)_3$ along the misfit axis. The structure has a composite layered structure with an *M*S block followed by a block of $[(NbS_2)_3]$. The *M*S block is a two-atom-thick layer with a distorted rock-salt structure. The Sn and the S are coordinated to five S and Sn atoms, respectively. The Sn has a square pyramidal geometry with four of the atoms

TABLE 4
Positional Parameters and Estimated Standard Deviations from the Refinement of the [SnS] Part (Space Group *Cm2a*)

Atom	Site	x	y	z	B or B_{eq} (Å²)[a]	sof
Sn1	4*c*	¼	0	0.4338(1)	2.10(4)	1.0
S4	4*c*	¾	0.966(2)	0.4516(3)	1.4(1)	1.0

Anisotropic Thermal Factors for Sn1[b]

Atom	U_{11}	U_{22}	U_{33}	U_{12}	U_{13}	U_{23}
Sn1	0.0034(1)	0.034(1)	0.0107(7)	0.0	0.0	0.004(5)

[a] The B_{eq} is defined as $B_{eq} = \frac{4}{3}(a^2B_{11} + b^2B_{22} + c^2B_{33})$.
[b] The anisotropic thermal factor is defined as $U = \exp[-2\pi^2\{h^2a^{*2}U_{11} + k^2b^{*2}U_{22} + l^2c^{*2}U_{33} + 2klb^*c^*U_{23}\}]$.

TABLE 5
Positional Parameters and Estimated Standard Deviations from the Refinement of the Common Part (Space Group *Cm2m*)

Atom	Site	x	y	z	B_{iso}	sof
Nb1	2*a*	—	0	0	0.25(5)	1.0
S1	4*c*	—	0.334	0.066	0.4(1)	1.0
Nb2	4*c*	—	0.333	0.253	0.29(3)	1.0
S2	4*c*	—	0.167	0.319	0.5(1)	1.0
S3	4*c*	—	0.167	0.187	0.5(1)	1.0
Nb supp	4*c*	—	0.002	0.137	0.5(3)	0.11
Sn1	4*c*	—	0.418(1)	0.4344(2)	2.5(1)	0.572(3)
S4	4*c*	—	0.383	0.452	4.5(7)	0.572

approximately in the same plane and one atom in the adjacent plane. The Sn–S bond distances in the plane range to 2.71 to 3.11 Å (see Table 6). The variation of the Sn–S bond distances in the plane is due to the slight shifting of the Sn and S atoms in the y direction. The Sn–S distance for the bond between the layers is 2.709 Å.

One layer in the $[(NbS_2)_3]$ part has the same structure as the early transition metal dichalcogenides. The Nb are sandwiched between two layers of S atoms. The Nb has a trigonal prismatic coordination of 6 S atoms. Due to the *Cm2m* space group symmetry, the middle layer is not related by symmetry to the other two layers whereas the two outer layers are related by symmetry. The average Nb–S bond distance in the trigonal prisms for all the layers is 2.47 Å (see Table 6). The distance is a typical Nb–S distance found in various polytypes of NbS_2 (9). The supplementary Nb in the van der Waals gap has octahedral coordination and shifts closer to one layer causing unequal Nb–S bond distances in the octahedron. The average Nb–S bond distance to the two outer NbS_2 layers is 2.25 Å while the average Nb–S bond distance to the middle layer is 2.54 Å. The shifting of the Nb minimizes the Nb–Nb repulsion between Nb1 and Nb supp. This shifting of the Nb in the van der Waals gap was also observed in the misfit compound "$PbNb_2S_5$" (2b).

This supplementary Nb is the probable cause of the stabilization of the trilayer material. As mentioned earlier, attempts to prepare the trilayer phase using only Sn was successful as confirmed by powder diffraction data. However, attempts to grow single crystal using I_2 transport resulted in the loss of SnS from the trilayer material. A small amount of Gd added to the reaction decreases the loss of SnS and then we are able to achieve crystallization.

As with the bilayered materials, the NbS_2 portion of the structure adopts a discernible polytype. One might expect to find a pure 3R polytype which is commonly found for NbS_2 and the misfit bilayer compounds. Figure 3 shows the projection of the 3R and $4H_a$ polytypes along the a axis. In the 3R polytype, the trigonal prisms for

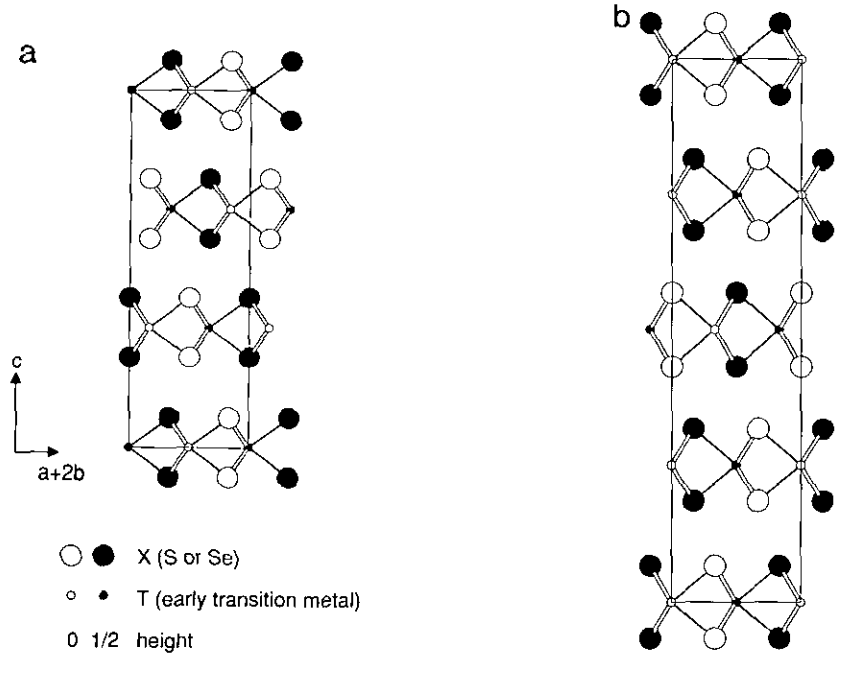

FIG. 3. The projection of (a) 3R and (b) $4H_a$ polytypes for the transition metal dichalcogenides shown along the a direction. In both polytypes, the metal atoms have trigonal prismatic coordination. In the 3R polytype, the trigonal prisms for each subsequent layer are oriented in the same direction. In the 4Ha polytype, three layers have the trigonal prisms oriented in the same direction with the fourth layer oriented in the opposite direction.

TABLE 6
Interatomic Distances (Å) for $(SnS)_{1.16}(NbS_2)_3$

SnS part

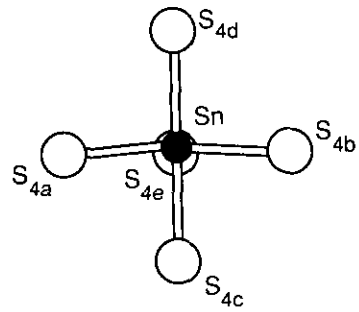

Sn1	–S4*a*	2.882(1)	
	–S4*b*	2.882(1)	
	–S4*c*	3.106(11)	
	–S4*d*	2.713(11)	
	–S4*e*	2.710(8)	
	$(Sn–S)_{ave}$ =	2.860	

NbS_2 part

Nb1	–2 × S1	2.475(3)	Interlayer (S–S) distances		
	–4 × S1	2.473(2)	S1	–S3	3.433(4)
Nb2	–1 × S2	2.477(4)			
	–2 × S2	2.474(2)			
	–1 × S3	2.471(4)	Nb supp	–Nb1	3.227(10)
	–2 × S3	2.467(3)		–Nb2	3.329(12)
	$(Nb–S)_{ave}$ =	2.473		–1 × S1	2.532(12)
				–2 × S1	2.545(9)
Intralayer (S–S) distances				–1 × S3	2.263(13)
S1	–S1	3.122(4)		–2 × S3	2.249(8)
S2	–S3	3.116(4)			

each layer of NbS_2 are oriented in the same direction. In the $4H_a$ three layers are oriented in the same direction and the fourth layer is oriented in the opposite direction. The NbS_2 portion in $(SnS)_{1.16}(NbS_2)_3$ also has three layers with the same orientation. Yet unlike the 3R–NbS_2, $(SnS)_{1.16}(NbS_2)_3$ has mirror plane in the middle of the $[(NbS_2)_3]$ layer similar to the $4H_a$ polytype. Therefore, this compound could be regarded as $\frac{3}{4}$ of the $4H_a$ polytype where the fourth layer of the polytype has been replaced by the *M*S layer.

The NbS_2 portion in the bilayered NbS_2 misfits has $\frac{2}{3}$ of the 3R polytype. The NbS_2 portion of the trilayer can also be described in a similar way. The middle layer of NbS_2 has $\frac{2}{3}$ of the 3R stacking in *y* direction with both the adjacent layers. This stacking then forms 2 connected portions of $\frac{2}{3}$ of the 3R–NbS_2 unit cell. The supplementary Nb in the Van der Waals gap also supports the variation of the 3R polytype. The chemical formulation for the refinement of NbS_2 portion is $Nb_{1+x}S_2$ where $x = 0.076$. This value of x is near the phase limit between 2H and 3R polytypes found for pure $Nb_{1+x}S_2$ (10). For the $Nb_{1+x}S_2$ system, the 3R polytype was observed when $x \geq 0.07$. With either description, the comparison to the $4H_a$ or 3R, $(SnS)_{1.16}(NbS_2)_3$ along with some of the bilayered misfits illustrate that a variety of polytypes are adopted by the misfits.

CONCLUSION

$(SnS)_{1.16}(NbS_2)_3$ is one of the first examples of a new type of misfit layered compound which has three consecutive layers of NbS_2. The misfit compounds in general can be described as intercalated materials where instead of ions or molecules an *M*S layer is located in the van der Waals gap. The monolayer misfits are first stage materials with alternate layers of *MX* and TX_2 layers. The bilayer misfits are second stage materials and this new trilayer material is a third stage material. Increasing the number of layers in the $[TX_2]$ portion of misfit compounds has interesting ramifications for the physical properties. The dependence of properties and staging has already been seen in the bilayered misfits and in the preliminary work on the Pb–Nb–Se compounds (3). For example, in the Pb–Nb–Se system, the superconducting temperature increases as the staging of the material increases. Also, the introduction of the van der Waals gaps provides an avenue for changing the physical properties and perhaps the structures of these higher stage materials through mechanical and chemical means.

REFERENCES

1. For a review of these materials, see G. A. Wiegers and A. Meerschaut *in* "Incommensurate Sandwiched Layered Compounds" (A. Meerschaut, Ed.), Trans. Tech. Publ. Ltd., Zürich, 1992.
2. (a) A. Meerschaut, L. Guemas, C. Auriel, and J. Rouxel, *Eur. J. Solid State Inorg. Chem.* **27,** 557 (1990); (b) C. Auriel, A. Meerschaut, and J. Rouxel, *Mater. Res. Bull.* **28,** 675 (1993); (c) C. Auriel, A. Meerschaut, R. Roesky, and J. Rouxel, *Eur. J. Solid State Inorg. Chem.* **29,** 1079 (1992); (d) R. Roesky, A. Meerschaut, and J. Rouxel, *Z. Anorg. Allg. Chem.* **619,** 117 (1993).
3. Y. Oosawa, Y. Gotoh, J. Akimoto, T. Tsunoda, M. Sohma and M. Onoda, *Jpn. J. Appl. Phys.* **31,** L1096 (1992).
4. P. Bonneau, P. Molinie, J-M. Grenêche and A. Meerschaut, unpublished results.
5. M. Evain, "U-FIT: A Cell Parameter Refinement Program." Institut des Matériaux, Nantes, France.
6. A. Meetsma, G. A. Wiegers, R. J. Haange, and J. L. DeBoer, *Acta Crystallogr. Sect. A* **45,** 285 (1989).
7. C. Kay Fair, MOLEN Software 2 (Enraf–Nonius), 1990.
8. N. Walker and D. Stuart, *Acta Crystallogr. Sect. A* **39,** 158 (1983).
9. (a) B. Morosin, *Acta Crystallogr. Sect. B* **30,** 551 (1974); (b) F. Jellinek, G. Brauer, and H. Müller, *Nature* **185,** 376 (1960).
10. W. G. Fisher and M. J. Sienko, *Inorg. Chem.* **19,** 39 (1980).